Hydrol. Earth Syst. Sci., 15, 1991–2005, 2011
www.hydrol-earth-syst-sci.net/15/1991/2011/
doi:10.5194/hess-15-1991-2011

Hydrology and Earth System Sciences

Anatomy of extraordinary rainfall and flash flood in a Dutch lowland catchment

C. C. Brauer[1], **A. J. Teuling**[1,*], **A. Overeem**[1,**], **Y. van der Velde**[1,2,***], **P. Hazenberg**[1], **P. M. M. Warmerdam**[1], **and R. Uijlenhoet**[1]

[1]Hydrology and Quantitative Water Management Group, Wageningen University, Wageningen, The Netherlands
[2]Soil Physics, Ecohydrology and Ground Water Management Group, Wageningen University, Wageningen, The Netherlands
[*]formerly at: Institute for Atmospheric and Climate Science, ETH Zurich, Zurich, Switzerland
[**]now at: Royal Netherlands Meteorological Institute, De Bilt, The Netherlands
[***]now at: Department of Physical Geography and Quaternary Geology, Stockholm University, Stockholm, Sweden

Received: 17 December 2010 – Published in Hydrol. Earth Syst. Sci. Discuss.: 11 January 2011
Revised: 31 May 2011 – Accepted: 15 June 2011 – Published: 27 June 2011

Abstract. On 26 August 2010 the eastern part of The Netherlands and the bordering part of Germany were struck by a series of rainfall events lasting for more than a day. Over an area of 740 km^2 more than 120 mm of rainfall were observed in 24 h. This extreme event resulted in local flooding of city centres, highways and agricultural fields, and considerable financial loss.

In this paper we report on the unprecedented flash flood triggered by this exceptionally heavy rainfall event in the 6.5 km^2 Hupsel Brook catchment, which has been the experimental watershed employed by Wageningen University since the 1960s. This study aims to improve our understanding of the dynamics of such lowland flash floods. We present a detailed hydrometeorological analysis of this extreme event, focusing on its synoptic meteorological characteristics, its space-time rainfall dynamics as observed with rain gauges, weather radar and a microwave link, as well as the measured soil moisture, groundwater and discharge response of the catchment.

At the Hupsel Brook catchment 160 mm of rainfall was observed in 24 h, corresponding to an estimated return period of well over 1000 years. As a result, discharge at the catchment outlet increased from 4.4×10^{-3} to nearly 5 m^3 s^{-1}. Within 7 h discharge rose from 5×10^{-2} to 4.5 m^3 s^{-1}.

The catchment response can be divided into four phases: (1) soil moisture reservoir filling, (2) groundwater response, (3) surface depression filling and surface runoff and (4) backwater feedback. The first 35 mm of rainfall were stored in the soil without a significant increase in discharge. Relatively dry initial conditions (in comparison to those for past discharge extremes) prevented an even faster and more extreme hydrological response.

1 Introduction

Flash floods, defined here as extreme floods generated by intense precipitation over rapidly responding catchments, have recently drawn increased attention, both from the scientific community and from the media. Their often devastating consequences, both in terms of material damage and loss of life, have triggered a number of European research projects (e.g. FLOODsite, HYDRATE, and IMPRINTS) to study the meteorological causes and hydrological effects of such events. These and other projects have lead to recent publications by e.g. Smith et al. (1996), Ogden et al. (2000), Gaume et al. (2003), Gaume et al. (2004), Delrieu et al. (2005) and Borga et al. (2007).

Correspondence to: C. C. Brauer
(claudia.brauer@wur.nl)

Published by Copernicus Publications on behalf of the European Geosciences Union.

From the perspective of water management and early warning, one of the main challenges posed by the phenomenon of flash floods is the extremely rapid response times of many of the catchments involved (as short as 10 min for certain small urban watersheds in mountainous environments). The consequence of this short lead time is that hydrological forecasting systems for regions with catchments prone to flash floods must rely heavily on meteorological forecasts, either from radar-based short-term precipitation forecasting (nowcasting) or from numerical weather prediction. Improved forecasting and early warning of flash floods is crucial, because the extreme discharges associated with such events (maximum specific discharges can reach tens of $m^3\,s^{-1}\,km^{-2}$) can have devastating societal consequences.

Typically, a timescale of a few hours is used to distinguish a flash flood from a regular flood. Since runoff generation is faster in mountainous catchments with steep slopes than in lowland catchments and since orography can impact the magnitude of rainfall extremes (Miglietta and Regano, 2008), most flash floods occur in mountainous areas. However in case of extreme rainfall, rapid runoff generation due to overland flow can also trigger flash floods in lowland catchments (Van der Velde et al., 2010).

Lowland areas, such as the densely populated delta region of The Netherlands, are typically associated with large-scale flooding of the Rhine and Meuse. These rivers have relatively slow response times (of the order of days to weeks). However, heavy rainfall events and the associated local flooding do occur in The Netherlands (Monincx et al., 2006). In addition, the magnitude of 24-h rainfall extremes that can trigger such flooding is expected to increase in a warmer climate (Kew et al., 2011). Thus, an improved understanding of the hydrological processes involved in the response of both natural and man made (polder) catchments to local heavy rainfall is needed to support water management in lowland areas.

In this paper we report on the flash flood triggered by an exceptionally heavy rainfall event on 26 August 2010 that occurred over the 6.5 km^2 Hupsel Brook catchment. The objective of this study is to understand the meteorological causes and hydrological effects of this event in order to improve process understanding and, eventually, flood forecasting models.

The catchment and available data will be described in Sect. 2, with special attention to the accuracy of the discharge measurements. We present a detailed analysis of the synoptic meteorological situation leading to the event (Sect. 3.1), the rainfall accumulations as measured by rain gauges, weather radar, and a microwave link (Sects. 3.2 and 3.3) and the extreme value statistics of the rainfall accumulation (Sect. 3.4). The soil moisture, groundwater and surface water response within the catchment will be described in Sects. 4.1–4.4. We present a dissection of the observed hydrological response into a sequence of contrasting regimes that characterize the storage and discharge dynamics of the catchment following this extraordinary rainfall event (Sect. 5). Finally we present our conclusions (Sect. 6)

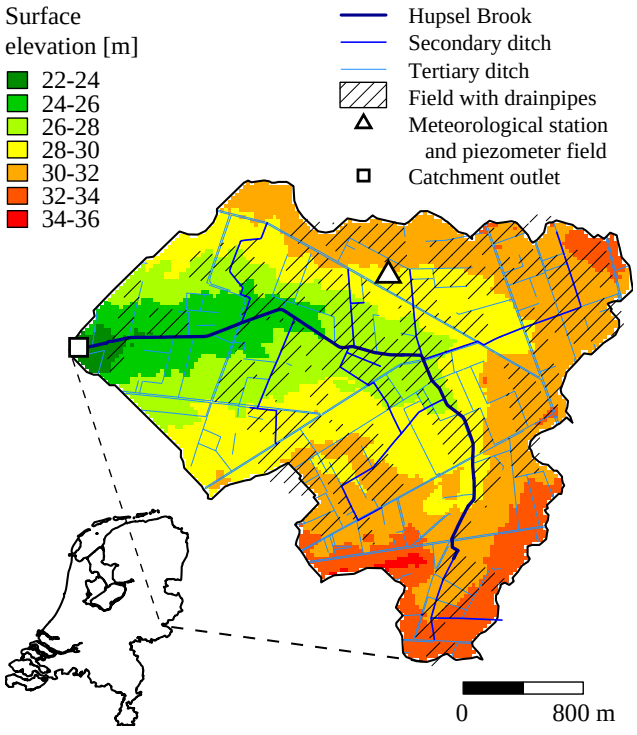

Fig. 1. Map of the Hupsel Brook catchment with the main hydrologically relevant features (adapted from Van der Velde et al., 2010).

2 Hupsel Brook experimental catchment

2.1 Field site

The Hupsel Brook catchment is situated in the east of The Netherlands (Fig. 1). Its area is 6.5 km^2, its elevation ranges from 22 to 35 m a.s.l. and the mean slope is 0.8 % (Van der Velde et al., 2009). The brook itself is 4 km long and has 7 small tributaries with lengths varying from 300 to 1500 m (Warmerdam, 1979). The slope of the brook is about 0.2 %. The land use is roughly 59 % grassland, 33 % agricultural (mostly maize), 3 % forest and 5 % built-on areas.

The Hupsel Brook catchment was selected as a research catchment in the 1960s because of its hydrogeological setting. The top layer consists of loamy sand with some clay, peat and gravel layers. Its thickness increases from 0.2 m in the east to 10 m in the west. The sand layer is situated on an impermeable marine clay layer of more than 20 m thickness. Consequently, there is one phreatic aquifer discharging to the brook and regional groundwater flow is assumed to be small.

The Hupsel Brook is of natural origin, but both the catchment and the brook have been modified by human intervention (Warmerdam, 1979). The meandering brook has been straightened and some trajectories have been restored. Many culverts have been constructed since the 1960s, which form potential obstacles during high flow conditions. Drainpipes have been installed in about 50 % of the plots (Fig. 1)

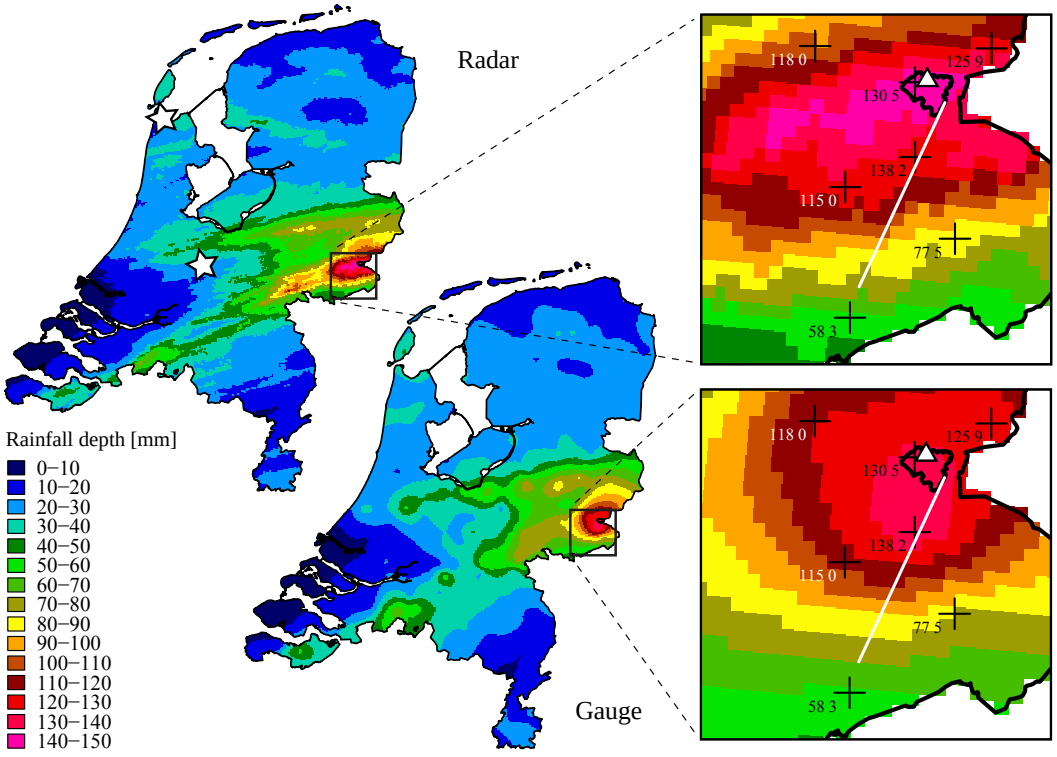

Fig. 2. Daily rainfall depths for 26 August, 08:00 UTC to 27 August, 08:00 UTC for The Netherlands and the region around the Hupsel Brook catchment. Upper panels: depths for the gauge-adjusted radar composite. Lower panels: depths for the interpolated manual rain gauge data. Also plotted are: weather radars (stars), manual rain gauges and their daily rainfall depths (plusses), automatic rain gauge (triangle), and microwave link path (line). Because the automatic rain gauge at Hupsel stopped recording at 21:00 UTC no daily rainfall depth was plotted for this gauge.

(Van der Velde et al., 2010). A dense network of ditches allows quick discharge when catchment storage is high, but the small (tertiary and secondary) ditches are often dry when catchment storage is low.

Since 1963 various hydrological, geological and meteorological measurement campaigns have been carried out in the Hupsel Brook catchment, which have been well documented in the literature (e.g., Colenbrander, 1965; Stricker and Brutsaert, 1978; Stricker and Warmerdam, 1982; Hopmans and van Immerzeel, 1988; Van Ommen et al., 1989; Hopmans and Stricker, 1989; Puente et al., 1993; Van der Velde et al., 2009; Rozemeijer et al., 2010). We refer to these studies for more information on the catchment.

2.2 Rainfall observations

The Royal Netherlands Meteorological Institute (KNMI) operates a network of 32 automatic meteorological stations (with a density of about 1 station per 1000 km^2), where rainfall (measured with an automatic rain gauge), global radiation and air temperature are measured (10-min resolution). One of the meteorological stations (called Hupsel) is located within the Hupsel Brook catchment (Figs. 1 and 2). Unfortunately, the rain gauge stopped recording at 26 August, 21:00 UTC, apparently due to instrumental problems caused by the exterme rainfall.

The KNMI also operates a manual rain gauge network (with a density of about 1 gauge per 100 km^2) to collect daily (08:00–08:00 UTC) rainfall accumulations. One of these manual rain gauges is located within the catchment, less than 1 km southwest of the meteorological station (Fig. 2).

Weather radars are valuable in flash flood research, because they give quantitative information about both the spatial and the temporal variability of rainfall (e.g. Bonnifait et al., 2009; Younis et al., 2008). Two weather radars are operated by the KNMI in De Bilt and Den Helder. The weather radar in De Bilt is about 100 km west of the catchment. Since standard weather radar rainfall estimates are prone to large errors, a network of 326 manual and 32 automatic rain gauges was used to adjust radar-based accumulations. This adjustment method has been described in detail and verified in Overeem et al. (2009a,b).

This extreme rainfall event provided a test-case for a less well-known source of rainfall data, which could be valuable in data-sparse regions or during extreme events. As part of commercial networks for mobile telecommunication, many microwave links have been installed in The Netherlands. Microwaves are sent from a transmitting antenna to a receiving

antenna. Rainfall attenuates the microwave signal and because of this, as a byproduct, such links can provide quantitative information about path-averaged rainfall intensities (Messer et al., 2006; Leijnse et al., 2007).

One of these microwave links has one antenna located within the Hupsel Brook catchment and the other 15.1 km to the southwest (see Fig. 2). From this link minimum and maximum received powers were available over 15-min intervals (with a resolution of 0.1 dB), based on 10-Hz sampling. The path-averaged rainfall intensity was estimated from the minimum and maximum received powers according to Overeem et al. (2011).

In the hydrological analysis 1-h rainfall data from the automatic rain gauge at the meteorological station in Hupsel have been used. When no automatic rain gauge data were available (between 26 August, 21:00 UTC and 27 August, 15:00 UTC) the gauge-adjusted 1-h radar rainfall depths at the same location have been used.

2.3 Groundwater and soil moisture observations

In a field (with drainpipes) located next to the meteorological station, 31 piezometers have been installed (Fig. 1) (Van der Velde et al., 2009). The surface has local elevations and depressions with height differences of about 50 cm. Here we use groundwater level data recorded with pressure sensors (resolution 15-min) from 2 representative piezometers: one in a local elevation and one in a local depression. A number of Echoprobe capacitance sensors (type Echoprobe EC-20) were also installed in this field to measure soil moisture content. Here we use data from one sensor at 40 cm depth situated in a local elevation.

We investigated the consequences of spatial variability in initial groundwater depths with the detailed groundwater model presented by Van der Velde et al. (2009). With this model a groundwater map was made for a day with similar measured groundwater levels at the piezometer field as on 25 August 2010 (namely 4 August 1994). With the groundwater depths from this map, potential saturation excess has been computed as the total rainfall depth minus groundwater depth times a specific storage of 10 %. These are potential values, because during the rainfall event, water is discharged to the brook or local depressions through the soil or drainpipes, leading to more saturation excess than computed near the brook and in local depressions. Spatial variation in rainfall and specific storage have not been taken into account when computing the potential saturation excess, but spatial variation in permeability and aquifer thickness have been incorporated in the model.

2.4 Discharge observations

Since 1968, discharge has been measured with a particular type of H-flume at the catchment outlet (Hooghart, 1984).

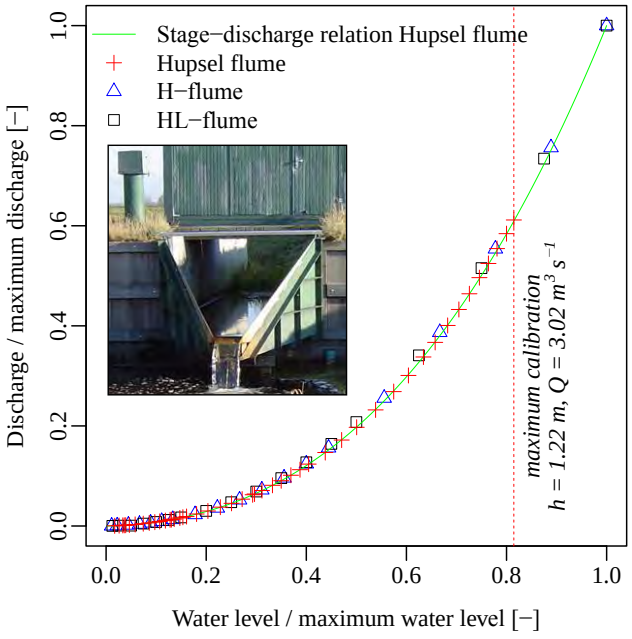

Fig. 3. Stage-discharge relationships for different types of H-flumes. Points: Calibration data of stage-discharge relationships of standard H- and HL-flumes and the flume at the outlet of the Hupsel Brook catchment. Line: The employed stage-discharge relationship for the Hupsel flume, extrapolated from $h = 1.22$ m. Water levels and discharges have been normalized with respect to their maximum values (Hupsel flume: $h_{max} = 1.50$ m, $Q_{max} = 4.94\,m^3\,s^{-1}$; H-flume: $h_{max} = 1.37$ m, $Q_{max} = 2.39\,m^3\,s^{-1}$; HL-flume: $h_{max} = 1.22$ m, $Q_{max} = 3.31\,m^3\,s^{-1}$). Calibration data of the H- and HL-flumes are taken from Kilpatrick and Schneider (1983). The inset shows the Hupsel flume.

Its temporal resolution for the period used in this paper was 15 min.

The flume at the catchment outlet is situated in a dam perpendicular to the brook with a higher level than the rim of the flume (Fig. 8). In post-event field surveys no evidence was found that water had flowed over the dam. Hence all water must have passed through the flume.

It is not likely that water levels in the flume rose higher than the measuring range of the stilling well. The maximum water height measured in the flume was 1.504 m, only 4 mm higher than the rim not yet reaching the bar, leading to a computed peak discharge of $4.98\,m^3\,s^{-1}$.

Because the flume is slightly narrower than a standard H-flume, the flume was calibrated in the Wageningen University hydraulics laboratory in 1969 and 1983 (Fig. 3). For low discharges a prototype was used and for high discharges a scale model. The flume was calibrated up to a water level of 1.22 m and corresponding discharge of $3.02\,m^3\,s^{-1}$. The obtained stage-discharge relationship was extrapolated to the maximum water level of 1.5 m, resulting in a discharge of $4.94\,m^3\,s^{-1}$.

Table 1. Overview of the post-event field surveys (photos in Fig. 8).

	Date	Activities
I	27 Aug, 06:00 UTC	Photographing
II	27 Aug, 13:00 UTC	General catchment inspection, instrument inspection, search for flood marks, interviews with inhabitants, photographing
III	29 Aug, 17:00 UTC	Photographing
IV	3 Sep, 10:00 UTC	General catchment inspection, instrument inspection, search for flood marks, groundwater data collection, photographing
V	13 Sep, 14:00 UTC	Photographing

To examine if such an extrapolation is valid, we compared laboratory experiments from our flume to those of standard H- and HL-flumes, which have been calibrated to the rim (Kilpatrick and Schneider, 1983). For each flume, water levels and discharges are normalized with respect to their maximum values and plotted against each other (Fig. 3). The deviations between the stage-discharge relationships of the different types of H-flumes were very small, from which we conclude that the employed extrapolation does not introduce significant errors.

During the second post-event field survey (see Sect. 2.5), the flume was found to be partially submerged (i.e., the water level downstream of the flume was higher than the crest of the flume). When flumes are submerged, water downstream of the flume introduces an additional resistance, leading to higher stage heights in the flume at a given discharge. When measured stage heights are used to compute discharges without accounting for (partial) submergence, the discharge will be overestimated.

Fortunately, H-flumes are not sensitive to submergence. When the submergence ratio (water level downstream of the flume divided by stage height, both with respect to the crest) of a standard H-flume is 50%, the stage height is overestimated by only 3 % (Brakensiek et al., 1979). A submergence ratio of 60 % leads to a stage height overestimation of 5 %. These values may differ slightly for the Hupsel flume. During post-event field survey II, the submergence ratio was estimated to be 56 % ($h_{\text{upstream}} = 1.23$ m and $h_{\text{downstream}} = 0.7$ m). This leads to an overestimation of the stage height by 4 % (based on data for H-flumes) and a possible overestimation of the discharge by 10 % (3.07 $\text{m}^3\,\text{s}^{-1}$ as an initial estimate and 2.80 $\text{m}^3\,\text{s}^{-1}$ after correction). During the peak, this effect might even have been smaller. Since we lack detailed information on downstream water levels, we assume that possible errors due to submergence are small enough to be neglected.

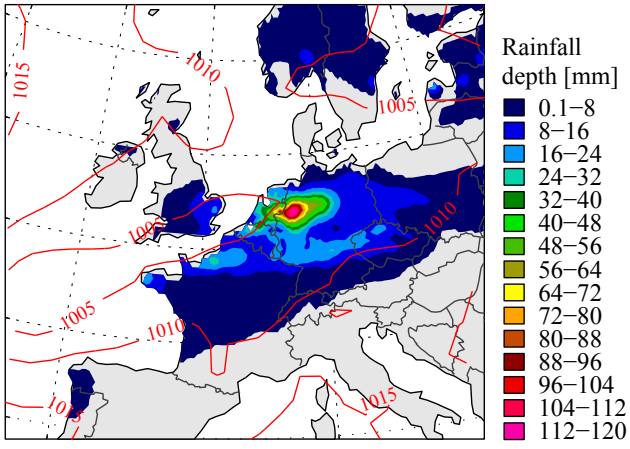

Fig. 4. Large-scale patterns of mean sea level pressure (hPa) and precipitation accumulation for 26 August 2010 (00:00–24:00 UTC). Pressure data come from the ERA Interim reanalysis (18:00 UTC). Precipitation is taken from the daily gridded observational dataset provided by the ECA & D (Haylock et al., 2008).

2.5 Post-event field surveys

Post-event field surveys can provide valuable information on water levels and flow processes in ungauged parts of the catchment (Gaume and Borga, 2008; Marchi et al., 2009). Such surveys were performed directly after the event on 27 August, as well as during several phases of the recession following the flash flood. During these surveys, photographs were taken on several locations in the catchment and all instrumentation was inspected. Additional information was provided by local inhabitants. A summary of the surveys is provided in Table 1.

3 Rainfall event

3.1 Synoptic situation and rainfall pattern

The synoptic chart at 26 August, 18:00 UTC shows an elongated region with multiple shallow low pressure centres stretching from the Bay of Biscay to Poland (Fig. 4). The low pressure centres were sandwiched between bands of high pressure over the north Atlantic and southern Europe, which allowed the system to remain stationary during most of the day. Because pressure gradients were small, wind speeds were low and storm cells moved slowly.

Along these low pressure centres a warm front was present, which divided warm, humid air in the south from cooler air in the north. The temperature gradients over The Netherlands were large. For example, a difference of 8 °C in maximum daily surface temperature was found over 150 km.

The frontal transition zone of warm air in the south and cooler air in the north of The Netherlands caused several active disturbances during 26 August. In the course of

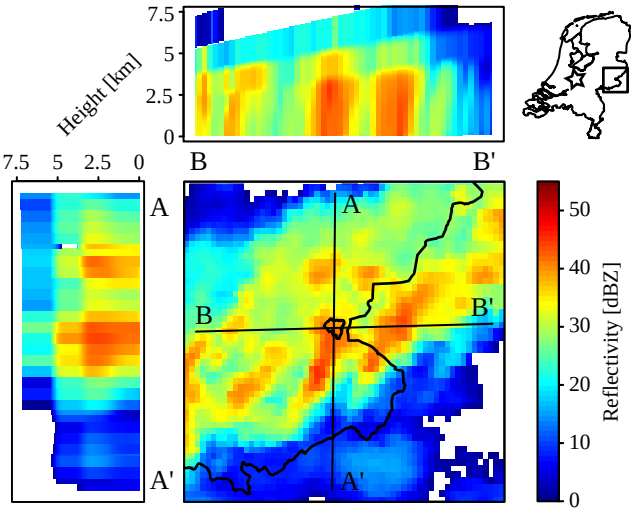

Fig. 5. Spatial variation in radar reflectivity for 26 August, 19:15 UTC. Reflectivity is derived from the 14-elevation volume scan of the KNMI weather radar in De Bilt (star). Side panels show the vertical distribution of the reflectivity for two transects over the Hupsel Brook catchment.

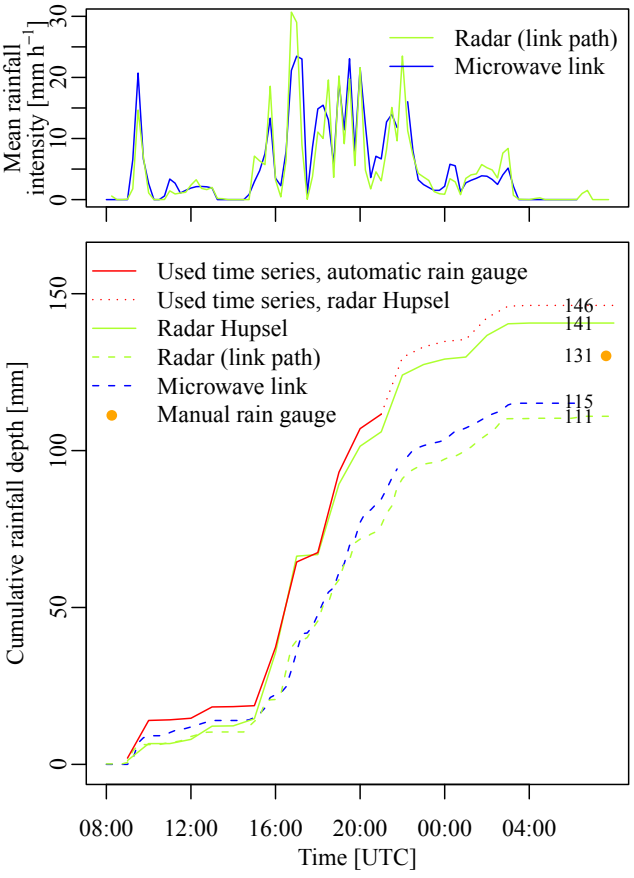

Fig. 6. Top: temporal dynamics of rainfall intensity. Blue: microwave link. Green: path-averaged gauge-adjusted radar data. The temporal resolution is 15 min. Rainfall intensities from radar data are shifted 15 min forward in time, because it takes some time for the droplets measured aloft by the radar to reach the level of the microwave link. Bottom: cumulative rainfall depths from 26 August, 08:00 UTC to 27 August, 08:00 UTC. Solid red: automatic rain gauge. Dotted red: gauge-adjusted radar data at the location of the automatic rain gauge, which were used to fill gaps of the automatic rain gauge data. Solid green: gauge-adjusted radar data at the location of the automatic rain gauge. Dashed green: gauge-adjusted radar data averaged over the microwave link path. Dashed blue: microwave link. One orange point: manual rain gauge.

the afternoon the atmosphere south of the warm front became unstable, giving rise to some very heavy, mostly convective rain showers in the middle and eastern part of the country. These disturbances were part of a mesoscale convective system and passed The Netherlands with a west-southwesterly flow, locally resulting in extraordinary accumulations of rainfall (see Schumacher and Johnson, 2005, for a description of a mesoscale convective system). Similar accumulations were recorded in parts of Northwestern Germany (Fig. 4).

Because storm cells moved along a stationary line, it rained continuously for long periods of time in several places. More than 18 h of near-continuous rainfall was recorded in De Bilt (the location of one of the employed KNMI weather radars).

The rainfall pattern which lead to these heavy intensities was highly variable, containing both convective and stratiform rainfall. Figure 5 presents a clear example of the spatial variability in the rainfall field as observed by the weather radar in De Bilt at 19:15 UTC. This weather radar scans at different elevation angles, which makes it possible to obtain a vertical profile of radar reflectivity (Hazenberg et al., 2011). In Fig. 5 both the horizontal and vertical extent of the convective area (reflectivity exceeding 40 dBZ) can be clearly identified.

The convective cells were part of a larger southwest-northeast oriented squall line that became apparent in the Hupsel Brook catchment at 15:30 UTC (see also Fig. 6). In this squall line new convective cells with heavy precipitation were generated upstream of the Hupsel Brook catchment until 22:15 UTC. This happens often in mesoscale convective systems and can lead to extreme rainfall accumulations (Schumacher and Johnson, 2008). The convective areas were highly variable in space, but many passed over the Hupsel Brook catchment. After 22:15 UTC rainfall became more stratiform.

3.2 Estimation using rain gauges and weather radar

Figure 2 shows daily rainfall depths for 26 August, 08:00 UTC to 27 August, 08:00 UTC for the gauge-adjusted radar composite and the interpolated manual rain gauge data. Locations of the manual rain gauges and their observed daily sums are also shown.

The highest manual rain gauge rainfall depth for this day (138 mm) was observed in Lievelde, 4 km southwest of the catchment. This, for Dutch conditions, extraordinary accumulation is among the highest ever recorded in The Netherlands since official registration of the national rain gauge network started in 1951. The highest daily rainfall depth measured (with manual rain gauges) since 1951 was 148 mm, the second highest 146 mm (source: KNMI). The 3rd, 5th and 7th places are occupied by Lievelde (138 mm), Hupsel (131 mm) and Rekken (126 mm) respectively, all from 26 August, 08:00 UTC to 27 August, 08:00 UTC (all plotted in Fig. 2). On 3 August 1948, 208 mm of rainfall was measured elsewhere in the Netherlands, but this event is not included in the official records because not all protocols were standardized in that period.

At the location of the automatic rain gauge in the catchment a gauge-adjusted radar rainfall depth of 141 mm was measured (08:00–08:00 UTC). Based on the data series from the automatic rain gauge (gaps filled with radar data), the maximum daily (08:00–08:00 UTC) rainfall depth is 146 mm and the maximum 24-h rainfall depth is 160 mm (04:00–04:00 UTC). This is larger than the largest 24-h rainfall depth observed in the 11-year climatological radar data set for the entire land surface of The Netherlands (142 mm for a radar pixel of 6 km^2).

Figure 6 shows that the cumulative rainfall depths from 26 August, 08:00 UTC to 26 August, 21:00 UTC from the automatic rain gauge and the gauge-adjusted radar hardly differ. Daily accumulations from radar and manual rain gauge are comparable, which is partly induced by the gauge-adjustment of the radar data. Temporal rainfall variations from radar and rain gauge (not induced by daily gauge-adjustment) are quite similar as well.

The rainfall event can be divided into roughly four parts according to rainfall intensity (see also Figs. 6 and 8). From 04:00 to 10:00 UTC rainfall was moderately intense (27 mm; mean rainfall intensity 5 mm h^{-1}), from 10:00 to 15:00 UTC rainfall was light (5 mm; mean rainfall intensity 1 mm h^{-1}), from 15:00 to 22:00 UTC rainfall was intense (111 mm; mean rainfall intensity 16 mm h^{-1}) and from 22 to 03:00 UTC rainfall was moderately intense (16 mm; mean rainfall intensity 3 mm h^{-1}).

The spatial extent (including a part of Germany) of the extreme event is derived for the largest 24-h rainfall depths (04:00–04:00 UTC) from the gauge-adjusted radar composite. The 24-h rainfall depth exceeds 100 mm for a 2100 km^2 area, 120 mm for a 740 km^2 area, and 140 mm for a 170 km^2 area. The scale of this event is considerably larger than the largest scale of the 24-h rainfall depth exceeding 100 mm, $\sim$450 km^2, as found in the 11-year climatological radar dataset for The Netherlands (Overeem et al., 2010).

3.3 Estimation using microwave link

During the event of 26 August, the microwave link connection remained stable 93 % of the time – high rainfall intensities did not cause instrumentation problems. The obtained depths correspond well to the radar depths measured over the same path (Fig. 6). The top panel in Fig. 6 shows that the dynamics of the link-based rainfall intensities are similar to those obtained from path-averaged gauge-adjusted radar rainfall intensities. This confirms that microwave links are a useful addition to the existing gauge networks and that they can be used to estimate rainfall in areas where no gauges are available.

This is a simple, first-order attempt to estimate rainfall intensities from this commercial microwave link: Some important sources of error were not taken into account: (1) there may be attenuation due to wet antennas, (2) mean rainfall intensities are simply calculated as the average of the minimum and maximum rainfall intensities, and (3) the large spatial rainfall variability, as indicated by Figs. 2 and 5, can cause overestimation for a link of this frequency (15.3 GHz) (Overeem et al., 2011).

3.4 Estimation of return period

While the rainfall event can easily be characterized as extraordinary based on the analysis in Sect. 3.2, the question remains what the occurrence probability of such an event is. Figure 7 shows a probability plot of 24-h rainfall depths, based on Overeem et al. (2008), who performed an extreme value analysis of rainfall depths from time series of 12 automatic rain gauges in The Netherlands (altogether 514 years of data). The concatenation of time series from the 12 stations to a single record of 514 years is justified according to Overeem et al. (2008). A rough estimate of the average return period of the 24-h rainfall depth for this event (based on automatic rain gauge and radar data), 160 mm (red square), is in the order of 6000 years for a given location.

When the extreme value analysis is repeated including the 160 mm rainfall depth, the average return period decreases to the order of 3000 years. Note that this hardly influences the quantiles of rainfall depths for average return periods up to about 100 years. Of course, these return periods are significantly larger than the return period of 160 mm being exceeded in 24 h at an arbitrary location in The Netherlands.

The uncertainties due to sampling variability have been shown to be large (Overeem et al., 2008). Using the bootstrap method the 95 % confidence interval was obtained. For the 24-h accumulation for a return period of 6000 years this interval ranges from 129 to 199 mm. Despite this large uncertainty, it is clear from Fig. 8 that the return period is well above 1000 years. The probability of such an event occurring at our experimental catchment between the start of the measurements in the 1960s and now is estimated to be about 0.8 %.

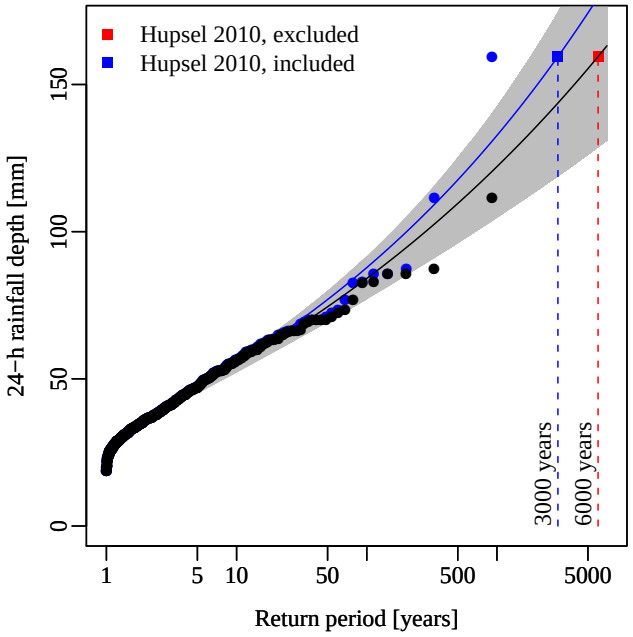

Fig. 7. Probability plot with the GEV distribution fitted to annual 24-h rainfall maxima. The method of L-moments was used (Hosking and Wallis, 1997). Black points: the 514 ordered annual maxima from Overeem et al. (2008) plotted with the Gringorten plotting position. Blue points: same data including the recent Hupsel maximum. Lines: GEV fits. Red and blue squares: The 24-h accumulation of 160 mm and corresponding return periods. Grey-shaded area: The 95 % confidence interval based on the bootstrap method.

4 Hydrologic response

4.1 Soil moisture response

When rainfall infiltrates into the unsaturated zone, soil moisture can be expected to react before groundwater and runoff. Figure 8 shows the observed local response of soil moisture content. Before the rainfall event, the soil was relatively dry. The soil moisture content measured by the available sensor at 40 cm depth was initially 23 % and started to rise at 27 August, 07:00 UTC, 3 h after the start of the rainfall event. As a result of the first part of the rainfall event with moderate intensities (04:00–09:00 UTC) the soil moisture content rose slowly to 32 % at 10:00 UTC. Between 09:00 and 10:00 UTC 12 mm of rainfall was recorded, leading to a steep increase in soil moisture content up to 41 % at 11:00 UTC. Between 10:00 and 12:00 UTC there was hardly any rainfall and the soil moisture content remained constant, but between 12:00 and 13:00 UTC another 3.6 mm of rainfall occurred and the soil moisture content reached saturation (45 %) at 14:30 UTC. After that, the soil moisture content slowly decreased, but remained above 40 % until 27 August, 19:30 UTC. The high soil moisture contents contributed to the strong groundwater table response. It should be noted that soil moisture contents returned to pre-event levels within 3 days.

4.2 Groundwater response

The depth and dynamics of the groundwater levels depend on the distance to ditches and drainpipes and on the microtopography (Van der Velde et al., 2010). In Fig. 8 groundwater depths are shown for 2 piezometers; one located in a local depression and one on a local elevation.

Initially, groundwater depths measured by two piezometers shown in Fig. 8 were 90 (depression) and 115 cm (elevation) below surface. Groundwater levels started to rise slowly at 11:30 UTC, more than 4.5 h after the initial increase in soil moisture content was observed. In the groundwater time series, the influence of single peaks in rainfall intensity is not visible. At 17:30 UTC, when groundwater levels were 48 and 88 cm below surface, groundwater rise accelerated. This was 7.5 h after the soil moisture content increase accelerated. Groundwater rise accelerated when soil moisture content increased, because less water could be stored in the unsaturated zone. In addition, rainfall intensity increased after 15:00 UTC and therefore more water was available to fill the pore spaces.

Around 20:15 UTC, the soil at the local depression became completely saturated and ponding occurred. Due to the larger available storage, it took until 22:45 UTC for the soil at the local elevation to become completely saturated. Ponding was less pronounced here likely due to water flowing into the local depressions. Because ponding did not occur, the groundwater level at the local elevations showed strong dynamics during and after rainfall events, while the groundwater level in the local depression remained above land surface for 6 days, with a maximum ponding depth of 11 cm. Similar ponding depths were also observed in the field during post-event field survey II, with many of the local depressions still filled.

During post-event field survey II, water was still flowing overland from the ponds in the fields to the ditches at several places. Overland flow is usually assumed to be of little importance in relatively flat areas, but can occur in lowland areas such as The Netherlands in case of high groundwater tables and/or high rainfall intensities (Appels et al., 2011). During post-event field survey II some farmers were seen digging small channels in the field to reduce ponding and transport the water to the ditches more quickly.

Uncertainty in interpreting these measurements arises mostly from sampling variability. Both soil moisture content and groundwater depth are highly variable in space. Therefore, these measurements do not provide the catchment representative soil moisture content or groundwater depth, but provide a mere indication of their local dynamics.

4.3 Spatial variation in saturation excess

The groundwater depth was on average 1559 mm before the rainfall event; a depth which is exceeded 96 % of the time. Because groundwater depths are not distributed uniformly

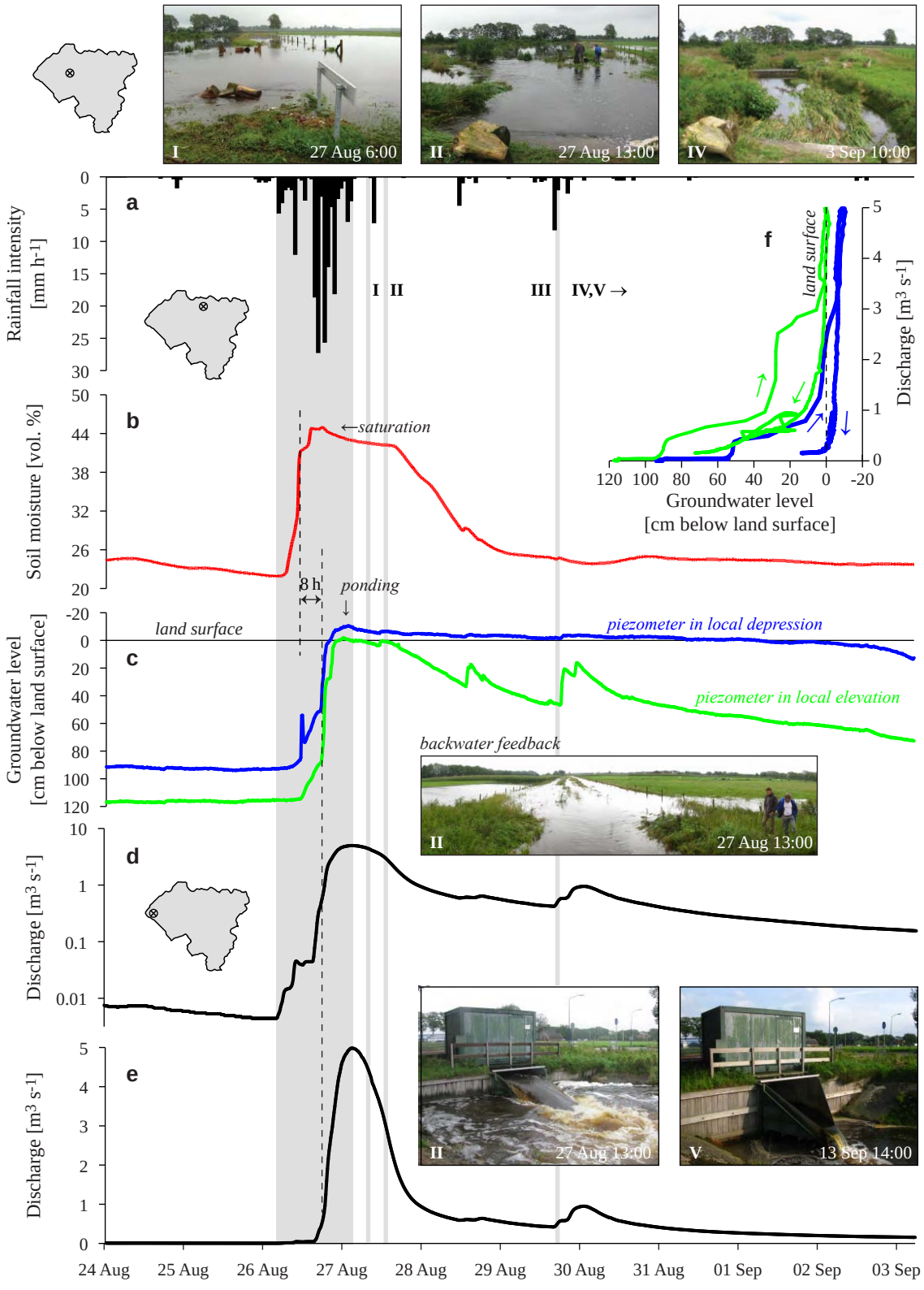

Fig. 8. Hydrological response of the Hupsel Brook catchment to the 26 August 2010 rainfall. **(a)** hourly rainfall depths measured with the automatic rain gauge (gaps filled with radar estimates), **(b)** soil moisture content at 40 cm depth, **(c)** groundwater level in two piezometers, **(d)–(e)** discharge at the catchment outlet on logarithmic and linear axes, and **(f)** relation between discharge and groundwater depth. The grey band indicates the rainfall period. The roman numbers and grey lines indicate the post-event field surveys (Table 1). The small catchment maps show (1) the location of the three upper photos, (2) the location of the rainfall, soil moisture and groundwater measurements and (3) the location of the catchment outlet and the three lower photos.

in the Hupsel Brook catchment, we used the model by Van der Velde et al. (2009) to create a map of potential saturation excess as a proxy for surface runoff generation (Fig. 9).

With spatially variable initial groundwater depths, 59 % of the catchment area is saturated at the end of the rain storm (after 160 mm). This has consequences for the mean saturation excess after 160 mm (4 mm for uniform or 11 mm for variable initial groundwater depths) and therefore for ponding and surface runoff.

In the southeastern part of the catchment, the aquifer is less thick and the permeability of the soil is lower, leading to shallower initial groundwater levels and therefore to higher potential saturation excess values (see Fig. 9). During post-event field survey II, we observed a high outflow at the sub-catchment outlet (circle in Fig. 9) which drains this part of the catchment. Because no measurement devices were installed at that weir, unfortunately no quantitative information is available.

4.4 Discharge response

Discharge showed little to no response to the first 35 mm of rainfall which were absorbed in the soil. Discharge started to rise slowly 7 h after the start of the rainfall event. Within 23 h, from 26 August 04:15 UTC to 27 August 02:45 UTC, discharge increased from 4.4×10^{-3} $m^3 s^{-1}$ to the maximum observed value of 4.98 $m^3 s^{-1}$, i.e., by more than three orders of magnitude. The discharge increased from 5.0×10^{-2} to 4.5 $m^3 s^{-1}$ in 7 h. The most spectacular rise took place on 26 August between 17:30 and 22:30 UTC, when discharge increased from 0.42 $m^3 s^{-1}$ to 4.0 $m^3 s^{-1}$.

Discharge remained above 1 $m^3 s^{-1}$ for 28 h and exceeded the 99th percentile (0.46 $m^3 s^{-1}$) for 4 days (Sect. 4.5). In Fig. 8e it seems that discharge has dropped to its pre-event level within days, but on a logarithmic scale (Fig. 8d) it can be seen that this would have taken weeks. On 3 September (at the end of the period shown in Fig. 8) discharge was still 0.15 $m^3 s^{-1}$; a value which is exceeded only 10 % of the time.

Between 26 August and 7 September, 184 mm of rainfall were recorded (by the automatic rain gauge, with data gaps filled with gauge-adjusted radar data). In the same period 92 mm were discharged, yielding a runoff ratio of 50 %. The other 50 % has been stored in the soil (∼70 mm) or has evaporated (20–25 mm).

There are some constructions in or around the brook which become obstacles in case of high discharges. The most important structures influencing the flow regime are the culverts. When discharge exceeds the design discharge of the culverts, a much larger head difference is needed between both sides of culvert, leading to floods upstream of the culvert in the brook or on the floodplain. Just 100 m upstream of the catchment outlet a culvert with a design discharge of about 5 $m^3 s^{-1}$ is located, which likely limited the discharge peak at the flume to about 5 $m^3 s^{-1}$.

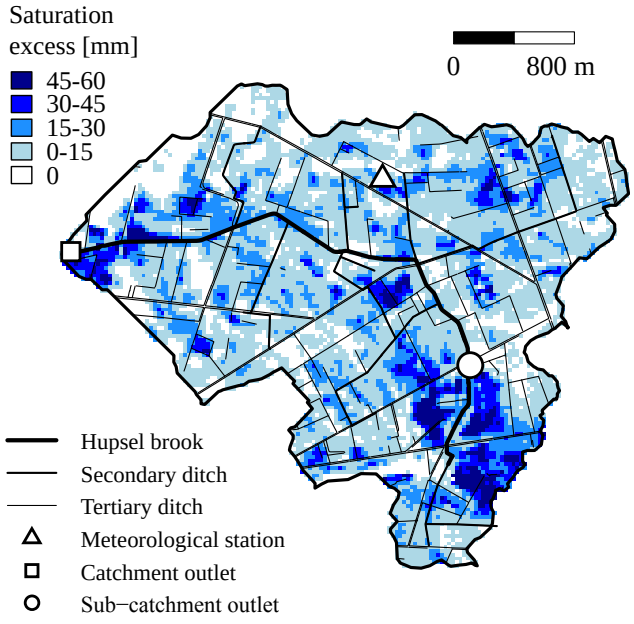

Fig. 9. Potential saturation excess, computed from the initial groundwater level, a specific storage of 10 % and the total amount of rainfall of 160 mm.

When catchment storage increases, the dense network of drainpipes and ditches becomes more important. Before the rainfall event, groundwater levels were below the level of drainpipes, tertiary ditches and most of the secondary ditches. The drainage network was therefore not fully used and water was mostly transported through the subsurface and therefore relatively slowly. When groundwater levels rose, drainpipes and ditches started to transport water, leading to an increase in discharge capacity and in discharge itself. Without this drainage network, ponding depths and the resulting damage would have been larger in the Hupsel Brook catchment.

The peak of 4.98 $m^3 s^{-1}$ corresponds to a specific discharge of 0.77 $m^3 s^{-1} km^{-2}$, or 2.8 $mm\ h^{-1}$, which is exceptional for a small catchment with an average slope of only 0.8 %. We applied the extreme value analysis of Sect. 3.4 to the discharge peak, using a Gumbel distribution. The 95 %-confidence interval of the highest discharge in the period 1969–2009, 21 $mm\ d^{-1}$ (return period of 98 years) is already large: 18–25 $mm\ d^{-1}$. Because of this, the relatively limited number of years for which discharge data are available prevent an accurate estimation of the return period of the peak discharge of 42 $mm\ d^{-1}$, which is almost twice as large.

4.5 Discharge regime and previous extreme discharges

It is relevant to put the 27 August discharge peak, as well as the conditions prior to 26 August, into historical perspective. Based on a time series of mean daily discharge from 1969 to 2010 some statistics have been computed. Mean discharge at the outlet of the Hupsel Brook catchment is 0.06 $m^3 s^{-1}$

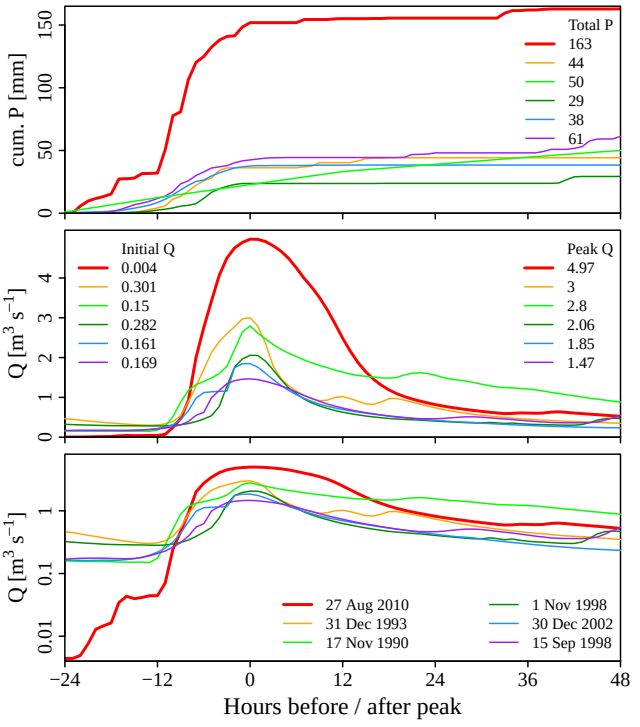

Fig. 10. Cumulative precipitation (top) and discharge on linear (middle) and logarithmic axis (bottom) of the six highest discharges since 1969.

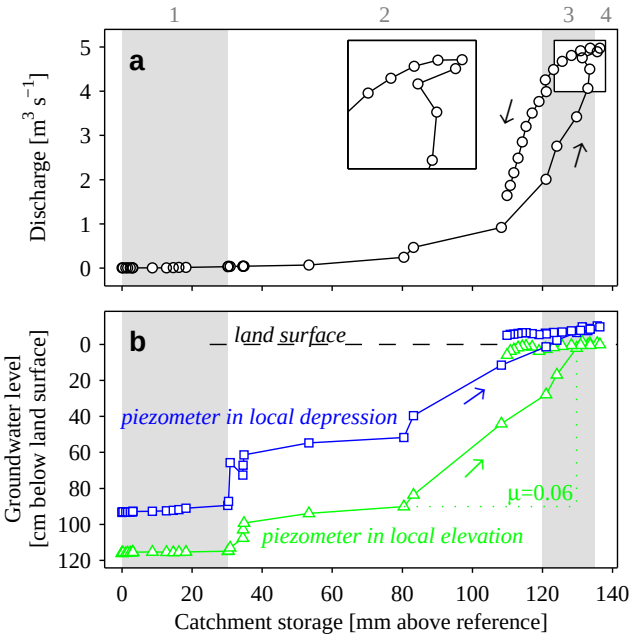

Fig. 11. Discharge at the outlet (upper panel) and local groundwater level (lower panel) as a function of estimated catchment storage for the period 25 August, 18:15 UTC to 27 August, 18:00 UTC. Points are drawn for each hour. The grey and white bands denote the four stages.

(0.8 mm d^{-1}). During 1 % of the time 0.17 m^3 s^{-1} is exceeded and during 0.1 % of the time 0.92 m^3 s^{-1} is exceeded. In the last decade of August (20–31 August), mean discharge is 0.016 m^3 s^{-1} and during 10 % of the time 0.043 m^3 s^{-1} is exceeded.

Sometimes there is no or hardly any discharge. During 10 % of the days in the last decade of August 1.1×10^{-3} m^3 s^{-1} is not reached. Before the start of this rainfall event, discharge was 4.4×10^{-3} m^3 s^{-1}, a value which is exceeded 81 % of the days overall and on 45 % of the days in the last decade of August. A discharge of 4.4×10^{-3} m^3 s^{-1} is therefore low in terms of the mean for the end of August, but it is not exceptional.

Since 1969, a daily mean discharge of 1 m^3 s^{-1} was exceeded six times (including this event). In Fig. 10 time series of cumulative precipitation and discharge are shown for these events. Compared to these previous events, the initial discharge on 26 August 2010 was about 50 times smaller. The low initial discharge and storage made it possible that a 4 times larger precipitation event led to "just" a 2 times larger discharge peak. The difference in initial discharge is clearly visible in the hydrograph on logarithmic y-axis (bottom). This graph also shows that on 26 August 2010 the first 78 mm of rainfall were used to increase the discharge to the initial discharge level of the previous events.

5 Synthesis of the hydrologic response

In many catchments, a close relation exists between the discharge at the outlet and the total amount of mobile water stored in the catchment (e.g., Kirchner, 2009; Teuling et al., 2010). While storage cannot be measured directly at the catchment scale, storage changes can be calculated by using the water balance over periods during which all fluxes are known. In case of the Hupsel flash flood, the contribution of evapotranspiration to the water balance is negligible around the discharge peak. Rainfall measured at the meteorological station may be considered representative for the whole 6.5 km^2 catchment. Hence, storage S can be calculated with respect to an arbitrary reference level S_0 by integrating the difference between rainfall R and discharge Q over time t:

$$S = S_0 + \int_{t=t_0}^{t} (R - Q)\,\mathrm{d}t. \quad (1)$$

In Fig. 11 both discharge and groundwater levels are plotted against total catchment storage as calculated by Eq. (1) for the period between 25 August 18:00 UTC and 27 August 18:00 UTC.

When interpreting the lines in Fig. 11 it should be noted that water can be stored in the catchment in different ways: (1) as soil moisture in the unsaturated zone, (2) as groundwater in the saturated zone, (3) as ponds in local depressions on the fields or (4) as surface water in the brook or on banks

and land surface in the floodplain. The subsequent filling of these storages, along with the interaction between them, ultimately determines the catchment response during the onset and peak of the flood. We hypothesize that the discharge dynamics at the catchment outlet reflects the following stages, each of which has a different sensitivity of discharge to storage changes:

1. *Soil moisture reservoir filling* – initially the upper part of the soil is dry, and rainfall is readily absorbed in the unsaturated zone. This leads to an increase in soil moisture content, but a lack of conductivity prevents groundwater levels from rising in conjunction with soil moisture. As a result, the discharge during this phase is hardly sensitive to storage changes up to a storage increase of ∼30 mm.

2. *Groundwater response* – the unsaturated zone is near saturation and additional rainfall readily leads to saturation of the soil matrix. Under these conditions the specific yield μ is very small (0.06 over a large part of the storage increase in Fig. 11) and groundwater levels can rise rapidly. Since groundwater levels strongly control the field-scale subsurface flow to the network of secondary and tertiary ditches, the discharge is moderately sensitive to changes in total catchment storage. The rapid rise of groundwater levels continues up to a storage increase of ∼120–130 mm, when groundwater levels reach the surface and ponding occurs.

3. *Surface depression filling and surface runoff* – when ponding occurs, two mechanisms come into play with contrasting effects on the discharge increase. First, the specific yield strongly increases (since for ponded areas $\mu = 1$), effectively reducing the increase in hydraulic heads in response to rainfall. Secondly, however, when ponds start to connect to the network of ditches, overland flow becomes an important runoff mechanism and discharge increases rapidly. This is a typical mechanism during flash floods, and the moment at which overland flow is initiated determines for a large part the timing of flash flood response (Marchi et al., 2010). This is also the case in the Hupsel Brook catchment. The slope of the line in Fig. 11a is very steep between total catchment storage of 120 mm and 135 mm. Measured groundwater levels indicate phreatic surfaces extending to above the local height of the land surface (which was confirmed by observations during post-event field surveys).

4. *Backwater feedback* – in the fourth phase discharge increases to above the design discharge of the culverts, leading to backwater feedbacks and extensive flooding of fields upstream of the culverts (Fig. 12). Such flooding was observed during post-event field surveys I and II (Fig. 8), especially in the area with elevations below 26 m (Fig. 1). The backwater effects strongly reduce the local pressure gradients that drive the flow of water through the subsurface. At the same time, they flatten the discharge peak. Figure 11 shows that high discharge levels persist during the decrease of the initial 20 mm of storage – consistent with the role of backwater.

Fig. 12. The role of culverts during the 27 August 2010 flash flood. The roman numbers indicate the post-event field surveys (Table 1). Upper panels: Situation directly after the flood. Upwelling water reveals the exit of the submerged culvert. The resulting backwater feedback allows water to bypass the obstacle on the right by flowing over the road and the adjacent field back into the brook (arrows). Lower left panel: upstream entry of the culvert. Logs (black arrows) deposited by flood and flow marks in grass (upper left panel) indicate that water flowed over the culvert at flood peak. Lower right panel: situation two weeks after flood with flood marks indicated. The photos in the top panels of Fig. 8 are taken from the same location as the photos in this figure, but in upstream rather than downstream direction.

Because initial groundwater levels, initial soil moisture contents, hydrogeology and land use vary spatially over the catchment, the timing of the different phases also varies spatially. During post-event field survey II more flooding was visible in the south-eastern part of the catchment, where the aquifer is thinner and groundwater levels shallower than in the western part. Therefore these phases cannot be separated exactly in Fig. 11. Nevertheless, these four stages appear to describe the observed hydrological response of the Hupsel Brook catchment to the extraordinary rainfall of 26 August 2010 well.

The stages resemble the stages identified by Maréchal et al. (2009), who described a flash flood response in a karstic area. Here, a first rainfall event only caused soil saturation but a second caused a flash flood due to overland flow. In addition, Maréchal et al. (2009) reported on backwater feedbacks at locations with limited discharge capacity.

We believe that because of the rapid increase in runoff during stage 3, in combination with the extremity of the rainfall,

the magnitude of the specific discharge peak, the local flooding and widespread surface runoff, this runoff event is best characterized as a lowland flash flood.

6 Conclusions

On 26 August 2010 the eastern part of The Netherlands was struck by a series of very heavy rainfall events leading to unprecedented peak discharges.

Rainfall was measured in the Hupsel Brook catchment with rain gauges (one automatic and one manual), a weather radar and a microwave link. The maximum 24-h rainfall depth was 160 mm. This rainfall depth corresponds to an estimated return period of more than 1000 years. The temporal dynamics of rainfall intensities measured by the microwave link compare well to those of radar rainfall intensities averaged over the path of the microwave link, which proves that this alternative source of rainfall data can be used in extreme situations. This may provide opportunities for poorly equipped catchments.

This rainfall event lead to a catchment response that is best described as a lowland flash flood, because of the extremity of the rainfall and the widespread surface runoff. Discharge at the catchment outlet increased from $4.4\times 10^{-3}\,m^3\,s^{-1}$ to nearly $5\,m^3\,s^{-1}$ (i.e. a specific discharge of $0.77\,m^3\,s^{-1}\,km^{-2}$, or $2.8\,mm\,h^{-1}$). Although this event was extreme, a detailed analysis has revealed that discharge has been measured relatively accurately.

We found that the catchment response can be divided in four stages:

1. *Soil moisture reservoir filling* – water is used to replenish soil moisture and discharge hardly rises.

2. *Groundwater response* – groundwater levels rise and discharge rises slowly.

3. *Surface depression filling and surface runoff* – ponds form in local depressions on the land surface, leading to surface runoff and rapid rise of discharge.

4. *Backwater feedback* – brook discharges exceed maximum discharge capacity of culverts in the brook. Water is stored behind the culverts, discharge hardly increases and local gradients that drive subsurface flow are reduced.

During this extreme event some thresholds became apparent that do not play a role during average conditions. Culverts hardly influence the rainfall-runoff characteristics in average situations, but become an important factor in case of high discharges, when discharges reach a ceiling and groundwater gradients are reduced. Often rainfall-runoff models are designed and calibrated with less extreme discharge data and then used to forecast peak flows. In these models, thresholds are not taken into account and as a consequence peak discharges are overestimated. Incorporation of such thresholds in hydrological models is currently being performed and shall be reported in future work.

Low initial catchment storage acted as a soil buffer and reduced the magnitude of the hydrologic response. The first 35 mm of rainfall were stored in the soil without a significant increase in discharge. Compared to the 5 highest discharge peaks since the 1960s, the initial discharge was 50 times smaller, which resulted in "just" a 2 times larger discharge peak after a 4 times larger rainfall event. These results show that for flood prediction, information on the initial hydrological state of the catchment can be as important as rainfall forecasts.

Acknowledgements. We thank Annemarie Braam (KNMI) for providing an internal report of the Weather Service department, which has been used in the description of the synoptic situation. We acknowledge the E-OBS dataset from the EU-FP6 project ENSEMBLES (http://ensembles-eu.metoffice.com) and the data providers in the ECA & D project (http://eca.knmi.nl). We thank KNMI for providing the radar and rain gauge data, T-Mobile Netherlands for the microwave link data, Deltares for groundwater and soil moisture data, Gert van den Houten (Water Board Rijn and IJssel) for the discharge data, ECMWF for ERA Interim data and Anton Dommerholt for the calibration data of the flume. We thank Jacqueline Meerink for providing photographs of the local flooding on 27 August, which helped us to assess the hydrologic response. A. J. Teuling acknowledges financial support from The Netherlands Organisation for Scientific Research through Veni Grant 016.111.002. P. Hazenberg and R. Uijlenhoet are financially supported by the EU-project IMPRINTS (FP7-ENV-2008-1-226555).

Edited by: M. Sivapalan

References

Appels, W. M., Bogaart, P. W., and van der Zee, S. E. A. T. M.: Influence of spatial variations of microtopography and infiltration on surface runoff and field scale hydrological connectivity, Adv. Water Resour., 34, 303–313, 2011.

Bonnifait, L., Delrieu, G., Le Lay, M., Boudevillain, B., Masson, A., Belleudy, P. Gaume, E., and Saulnier, G.: Distributed hydrologic and hydraulic modelling with radar rainfall input: Reconstruction of the 8–9 September 2002 catastrophic flood event in the Gard region, France, Adv. Water Resour., 32, 1077–1089, 2009.

Borga, M., Boscolo, P., Zanon, F., and Sangati, M.: Hydrometeorological analysis of the 29 August 2003 flash flood in the Eastern Italian Alps, J. Hydrometeorol., 8, 1049–1067, 2007.

Brakensiek, D., Osborn, H., and Rawls, W.: Field manual for research in agricultural hydrology, vol. 224 of Agricultural Handbook, US Department of Agriculture, 1979.

Colenbrander, H.: The research watershed "Leerinkbeek", Netherland, in: IAHS Red Book, vol. 66-II, 558–563, 1965.

Delrieu, G., Ducrocq, V., Gaume, E., Nicol, J., Payrastre, O., Yates, E., Kirstetter, P.-E., Andrieu, H., Ayral, P.-A., Bouvier, C., Creutin, J.-D., Livet, M., Anquetin, S., Lang, M., Neppel, L., Obled, C., Parent-du-Châtelet, J., Saulnier, G.-M., Walpersdorf, A., and Wobrock, W.: The catastrophic flash-flood event of 8–9 September 2002 in the Gard region, France: a first case study for the Cévennes-Vivarais Mediterranean Hydrometeorological Observatory, J. Hydrometeorol., 6, 34–52, 2005.

Gaume, E. and Borga, M.: Post-flood field investigations in upland catchments after major flash floods: proposal of a methodology and illustrations, J. Flood Risk Manage., 1, 175–189, 2008.

Gaume, E., Livet, M., and Desbordes, M.: Study of the hydrological processes during the Avène River extraordinary flood (south of France): 6–7 October 1997, Phys. Chem. Earth, 28, 263–267, 2003.

Gaume, E., Livet, M., Desbordes, M., and Villeneuve, J. P.: Hydrological analysis of the river Aude, France, flash flood on 12 and 13 November 1999, J. Hydrol., 286, 135–154, 2004.

Haylock, M., Hofstra, N., Klein Tank, A., Klok, E., Jones, P., and New, M.: A European daily high-resolution gridded dataset of surface temperature and precipitation, J. Geophys. Res.-Atmos., 113, D20119, doi:10.1029/2008JD010201, 2008.

Hazenberg, P., Leijnse, H., and Uijlenhoet, R.: Radar rainfall estimation of stratiform winter precipitation in the Belgian Ardennes, Water Resour. Res., 47, W02507, doi:10.1029/2010WR009068, 2011.

Hooghart, J.: Comparison of models for the unsaturated groundwater system and evapotranspiration, Report of the 4th CHO-study meeting in cooperation with the Study Group Hupsel Brook, Tech. Rep. 13, Commission for Hydrological Research TNO, in Dutch, 1984.

Hopmans, J. W. and Stricker, J. N. M.: Stochastic analysis of soil water regime in a watershed, J. Hydrol., 105, 57–84, 1989.

Hopmans, J. and van Immerzeel, C.: Variation in evapotranspiration and capillary rise with changing soil profile characteristics, Agr. Water Manage., 13, 295–305, 1988.

Hosking, J. and Wallis, J.: Regional Frequency Analysis: an Approach Based on L-moments, Cambridge University Press, Cambridge, 1997.

Kew, S. F., Selten, F. M., Lenderink, G., and Hazeleger, W.: Robust assessment of future changes in extreme precipitation over the Rhine basin using a GCM, Hydrol. Earth Syst. Sci., 15, 1157–1166, doi:10.5194/hess-15-1157-2011, 2011.

Kilpatrick, F. and Schneider, V.: Use of flumes in measuring discharge, vol. 3 of US Geological Survey Techniques of Water-Resources Investigations, Chap. A14, US Department of the Interior, 1983.

Kirchner, J.: Catchments as simple dynamical systems: catchment characterization, rainfall-runoff modeling, and doing hydrology backwards, Water Resour. Res., 45, W02429, doi:10.1029/2008WR006912, 2009.

Leijnse, H., Uijlenhoet, R., and Stricker, J. N. M.: Rainfall measurement using radio links from cellular communication networks, Water Resour. Res., 43, W03201, doi:10.1029/2006WR005631, 2007.

Marchi, L., Borga, M., Preciso, E., Sangati, M., Gaume, E., Bain, V., Delrieu, G., Bonnifait, L., and Pogačnik, N.: Comprehensive post-event survey of a flash flood in Western Slovenia: observation strategy and lessons learned, Hydrol. Process., 23, 3761–3770, 2009.

Marchi, L., Borga, M., Preciso, E., and Gaume, E.: Characterisation of selected extreme flash floods in Europe and implications for flood risk management, J. Hydrol., 394, 118–133, 2010.

Maréchal, J., Ladouche, B., and Dorfliger, N.: Hydrogeological analysis of groundwater contribution to the 6–8 September 2005 flash flood in Nîmes, Houile Blanche, in French, 88–93, 2009.

Messer, H., Zinevich, A., and Alpert, P.: Environmental monitoring by wireless communication networks, Science, 312, 713, 2006.

Miglietta, M. M. and Regano, A.: An observational and numerical study of a flash-flood event over south-eastern Italy, Nat. Hazards Earth Syst. Sci., 8, 1417–1430, doi:10.5194/nhess-8-1417-2008, 2008.

Monincx, S., Termes, P., and Tromp, G.: Management discharge peaks necessary to avoid problems with the Overijsselse Vecht, H_2O, in Dutch, 23, 44–47, 2006.

Ogden, F. L., Sharif, H. O., Senarath, S. U. S., Smith, J. A., Baeck, M. L., and Richardson, J. R.: Hydrologic analysis of the Fort Collins, Colorado flash flood of 1997, J. Hydrol., 228, 82–100, 2000.

Overeem, A., Buishand, A., and Holleman, I.: Rainfall depth-duration-frequency curves and their uncertainties, J. Hydrol., 348, 124–134, 2008.

Overeem, A., Buishand, A., and Holleman, I.: Extreme rainfall analysis and estimation of depth-duration-frequency curves using weather radar, Water Resour. Res., 45, W10424, doi:10.1029/2009WR007869, 2009a.

Overeem, A., Holleman, I., and Buishand, A.: Derivation of a 10-year radar-based climatology of rainfall, J. Appl. Meteorol. Clim., 48, 1448–1463, 2009b.

Overeem, A., Buishand, A., Holleman, I., and Uijlenhoet, R.: Extreme value modeling of areal rainfall from weather radar, Water Resour. Res., 46, W09514, doi:10.1029/2009WR008517, 2010.

Overeem, A., Leijnse, H., and Uijlenhoet, R.: Measuring urban rainfall using microwave links from commercial cellular communication networks, Water Resour. Res., submitted, 2011.

Puente, C. E., Bierkens, M. F. P., Diaz-Granados, M. A., Dik, P. E., and López, M. M.: Practical use of analytically derived runoff models based on rainfall point processes, Water Resour. Res., 29, 3551–3560, 1993.

Rozemeijer, J., van der Velde, Y., van Geer, F., Bierkens, M., and Broers, H.: Direct measurements of the tile drain and groundwater flow route contributions to surface water contamination: from field-scale concentration patterns in groundwater to catchment-scale surface water quality, Environ. Pollut., 158, 3571–3579, 2010.

Schumacher, R. and Johnson, R.: Organization and environmental properties of extreme-rain-producing mesoscale convective systems, Mon. Weather Rev., 133, 961–976, 2005.

Schumacher, R. and Johnson, R.: Mesoscale processes contributing to extreme rainfall in a midlatitude warm-season flash flood, Mon. Weather Rev., 136, 3964–3986, 2008.

Smith, J. A., Baeck, M. L., Steiner, M., and Miller, A. J.: Catastrophic rainfall from an upslope thunderstorm in the central Appalachians: the Rapidan storm of June 27, 1995, Water Resour. Res., 32, 3099–3113, 1996.

Stricker, J. and Brutsaert, W.: Actual evapotranspiration over a summer in the Hupsel Catchment, J. Hydrol., 39, 139–157, 1978.

Stricker, J. N. M. and Warmerdam, P. M. M.: Estimation of the water balance in the Hupselse Beek basin over a period of three years and a first effort to simulate the rainfall-runoff process for a complete year, in: Proceedings of the International Symposium on Hydrological Research Basins and Their Use in Water Resources Planning, Bern, Switzerland, 79–388, 1982.

Teuling, A. J., Lehner, I., Kirchner, J. W., and Seneviratne, S. I.: Catchments as simple dynamical systems: Experience from a Swiss prealpine catchment, Water Resour. Res., 46, W10502, doi:10.1029/2009WR008777, 2010.

Van der Velde, Y., de Rooij, G. H., and Torfs, P. J. J. F.: Catchment-scale non-linear groundwater-surface water interactions in densely drained lowland catchments, Hydrol. Earth Syst. Sci., 13, 1867–1885, doi:10.5194/hess-13-1867-2009, 2009.

Van der Velde, Y., Rozemeijer, J., de Rooij, G., van Geer, F., and Broers, H.: Field scale measurements for separation of catchment discharge into flow route contributions, Vadose Zone J., 9, 25–35, 2010.

Van Ommen, H., Dijksma, R., Hendrickx, J., Dekker, L., Hulshof, J., and van den Heuvel, M.: Experimental assessment of preferential flow paths in a field soil, J. Hydrol., 105, 253–262, 1989.

Warmerdam, P.: Hydrological effects of drainage improvement in the Hupselse Beek catchment area in the Netherlands, Tech. Rep. 64, Department of Hydraulics and Catchment Hydrology, Agricultural University, Wageningen, The Netherlands, 1979.

Younis, J., Anquetin, S., and Thielen, J.: The benefit of high-resolution operational weather forecasts for flash flood warning, Hydrol. Earth Syst. Sci., 12, 1039–1051, doi:10.5194/hess-12-1039-2008, 2008.